Additional Figures and Data

This document provides additional data and figures for the paper "Why heterogeneous cloud particles matter: Iron-bearing species and cloud particle morphology affects exoplanet transmission spectra". The parameters used for the calculation of the transmission spectra are shown in Table 1. The cloud particle opacities are listed in Table 2.

References

Begemann, B., Dorschner, J., Henning, T., et al. 1997, ApJ, 476, 199

Carone, L., Lewis, D. A., Samra, D., Schneider, A. D., & Helling, C. 2023, ArXiv, 2301.08492

Dorschner, J., Begemann, B., Henning, T., Jaeger, C., & Mutschke, H. 1995, A&A, 300, 503

Henning, T., Begemann, B., Mutschke, H., & Dorschner, J. 1995, A&A Supplement Series, 112, 143

Huffman, D. R. & Wild, R. L. 1967, Physical Review, 156, 989

Khachai, H., Khenata, R., Bouhemadou, A., et al. 2009, Journal of Physics: Condensed Matter, 21, 095404

Kiefer, S., Bach-Møller, N., Samra, D., et al. 2024, A&A, submitted

Kitzmann, D. & Heng, K. 2018, MNRAS, 475, 94

Kumar, A., Kumar, M., & Singh, R. P. 2021, Optik, 241, 167064

Montaner, A., Galtier, M., Benoit, C., & Bill, H. 1979, Physica Status Solidi Applied Research, 52, 597

Palik, E. D. 1985, Academic Press Handbook Series, New York: Academic Press, 1985, edited by Palik, Edward D.

Posch, T., Kerschbaum, F., Fabian, D., et al. 2003, ApJ Supplement Series, 149, 437

Querry, M. R. 1998, Optical Constants of Minerals and Other Materials from the Millimeter to the Ultraviolet (Chemical Research, Development & Engineering Center, U.S. Army Armament Munitions Chemical Command)

Suto, H., Sogawa, H., Tachibana, S., et al. 2006, MNRAS, 370, 1599

Zeidler, S., Posch, T., & Mutschke, H. 2013, A&A, 553, A81

Zeidler, S., Posch, T., Mutschke, H., Richter, H., & Wehrhan, O. 2011, A&A, 526, A68

Zubko, V. G., Mennella, V., Colangeli, L., & Bussoletti, E. 1996, MNRAS, 282, 1321

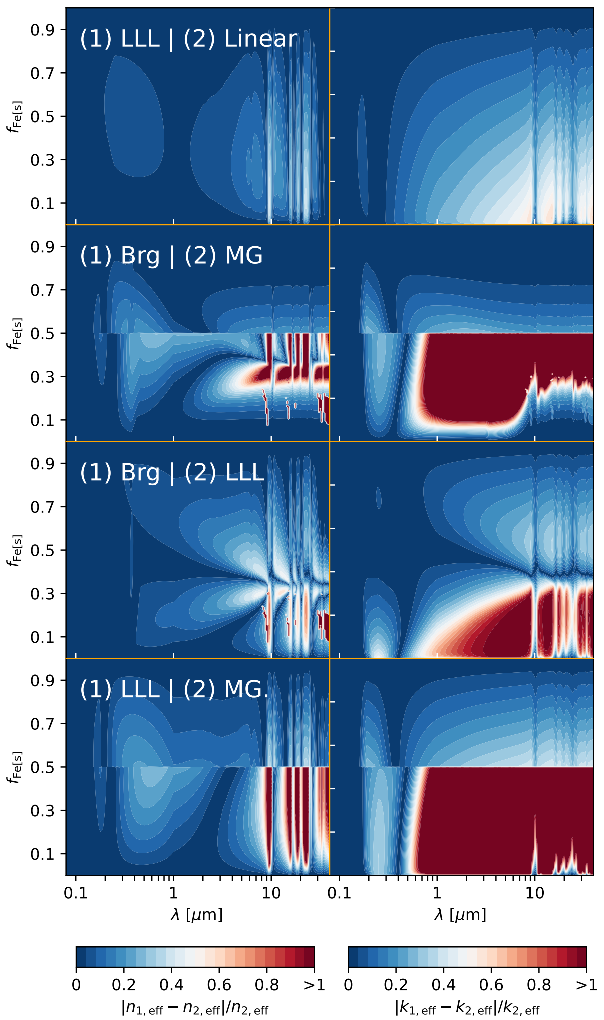

Fig. 1. Relative differences in the effective refractive index for the two-component material {Fe[s], Mg_2SiO_4[s]}. Compared are LLL, Bruggeman (Brg), Maxwell-Garnett (MG), and Linear.

Table 1. Planetary parameters and model details for the exoplanets used in this study.

	HATS-6b	WASP-39b	WASP-76b	WASP-107b
Planetary Radius R_{pl} [R_{jup}]	0.998	1.279	1.83	0.94
Gravitational acceleration g [cm^2 s^{-1}]	794	426	681	260
Stellar Radius R_{star} [R_{sun}]	0.57	0.932	1.73	0.66
Nucleating species				
TiO_2	✓	✓	✓	-
SiO	✓	✓	✓	-
NaCl	✓	✓	✓	-
KCl	✓	✓	✓	-
Cloud particle materials				
TiO_2[s]	✓	✓	✓	-
Al_2O_3[s]	✓	✓	✓	-
$CaTiO_3$[s]	✓	✓	✓	-
SiO[s]	✓	✓	✓	✓
SiO_2[s]	✓	✓	✓	✓
MgO[s]	✓	✓	✓	-
Fe[s]	✓	✓	✓	-
FeO[s]	✓	✓	✓	-
FeS[s]	✓	✓	✓	-
Fe_2O_3[s]	✓	✓	✓	-
Fe_2SiO_3[s]	✓	✓	✓	-
$MgSiO_3$[s]	✓	✓	✓	✓
$CaSiO_3$[s]	✓	✓	✓	-
Mg_2SiO_4[s]	✓	✓	✓	-
NaCl[s]	✓	✓	✓	-
KCl[s]	✓	✓	✓	-
$C_{amorphous}$[s]	-	-	-	✓

Table 2. References for the refractive indices of the cloud particle materials.

Material species	Wavelength range (μm)	Reference
Al_2O_3[s] (grass)	0.10 - 200	Begemann et al. (1997)
C[s] (graphite)	0.2 - 794	Palik (1985)
$C_{amorphous}$[s]	0.05 - 10000	Zubko et al. (1996)
$CaTiO_3$[s] (amorphous)	2 - 5843	Posch et al. (2003)
Fe[s] (metallic)	0.00012 - 285	Palik (1985)
FeO[s] (amorphous)	0.20 - 500	Henning et al. (1995)
Fe_2O_3[s] (amorphous)	0.10 - 1000	Amaury H.M.J. Triaud (unpublished)
Fe_2SiO_4[s] (amorphous)	0.20 - 500	Dorschner et al. (1995)
FeS[s] (amorphous)	0.10 - 100000	Henning (unpublished)
KCl [s] (cubic)	0.01 - 166	Palik (1985); Querry (1998)
$MgSiO_3$[s] (grass)	0.20 - 500	Dorschner et al. (1995)
Mg_2SiO_4[s] (crystalline)	0.10 - 1000	Suto et al. (2006)
MgO[s] (Cubic)	0.017 - 625	Palik (1985)
MnS[s]	0.01 - 190	Huffman & Wild (1967); Montaner et al. (1979)
MnO[s]	0.1 - 11	Kumar et al. (2021)
NaCl [s] (cubic)	0.05 - 166	Palik (1985); Querry (1998)
Na_2S[s]	0.05 - 200	Montaner et al. (1979); Khachai et al. (2009)
SiO_2[s] (alpha-Quartz)	0.00012 - 10000	Palik (1985), Zeidler et al. (2013)
SiO[s] (polycrystalline)	0.0015 - 14	Philipp in Palik (1985)
TiO_2[s] (Rutile)	0.47 - 36	Zeidler et al. (2011)
ZnS[s]	0.02 - 280	Palik (1985)

Notes. Data for KCl[s], ZnS[s], MnS[s], Na_2S[s], and NaCl[s] is taken from Kitzmann & Heng (2018).

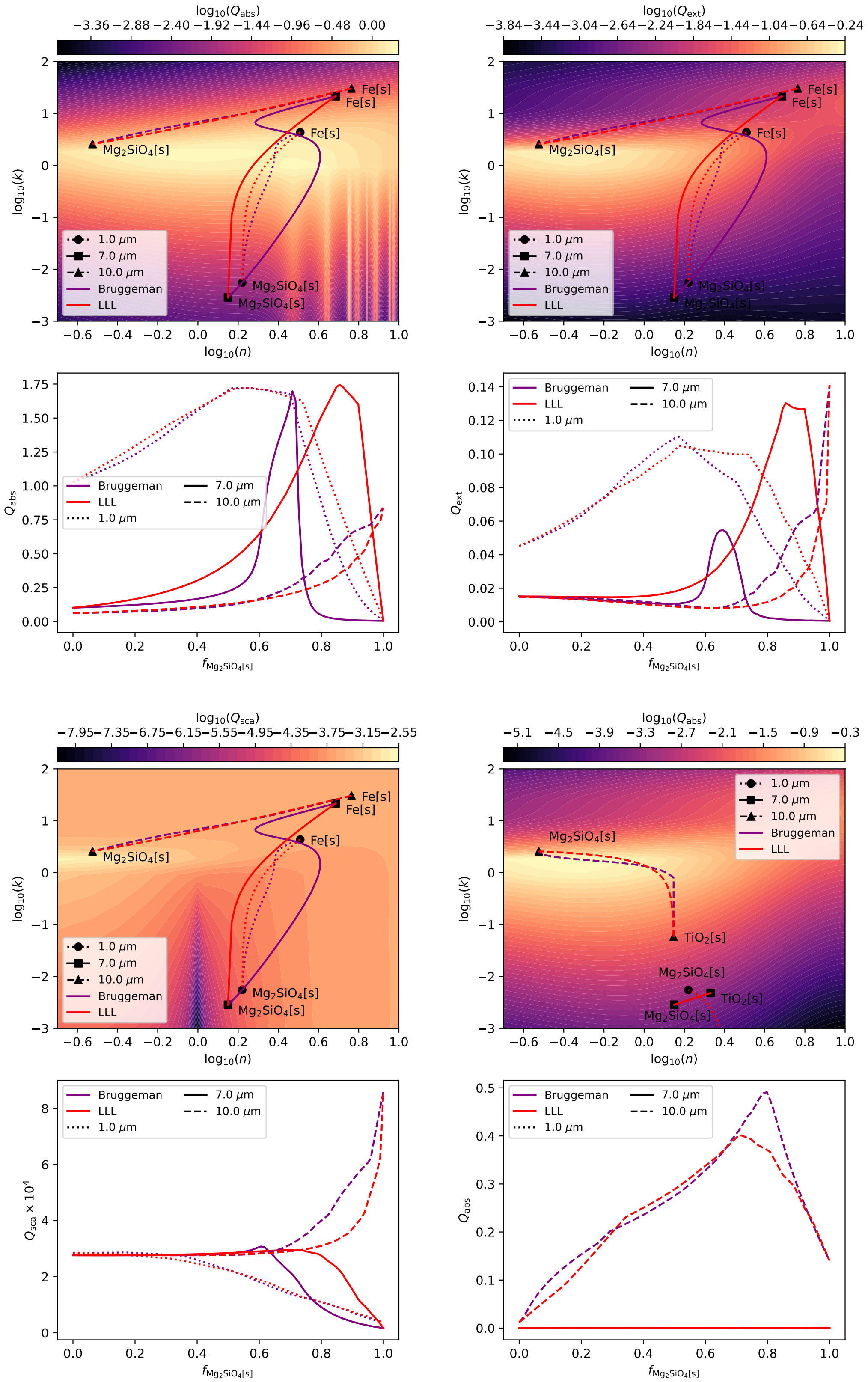

Fig. 2. Analysis of cloud particle optical property of two component materials. All set-ups are the same as in Sect. **??** except for the differences stated here. **Top left:** size parameter of $x = 1$. **Top right:** extinction efficiency instead of absorption efficiency. **Bottom left:** scattering efficiency instead of absorption efficiency. **Bottom right:** two component material $\{TiO_2[s], Mg_2SiO_4[s]\}$.

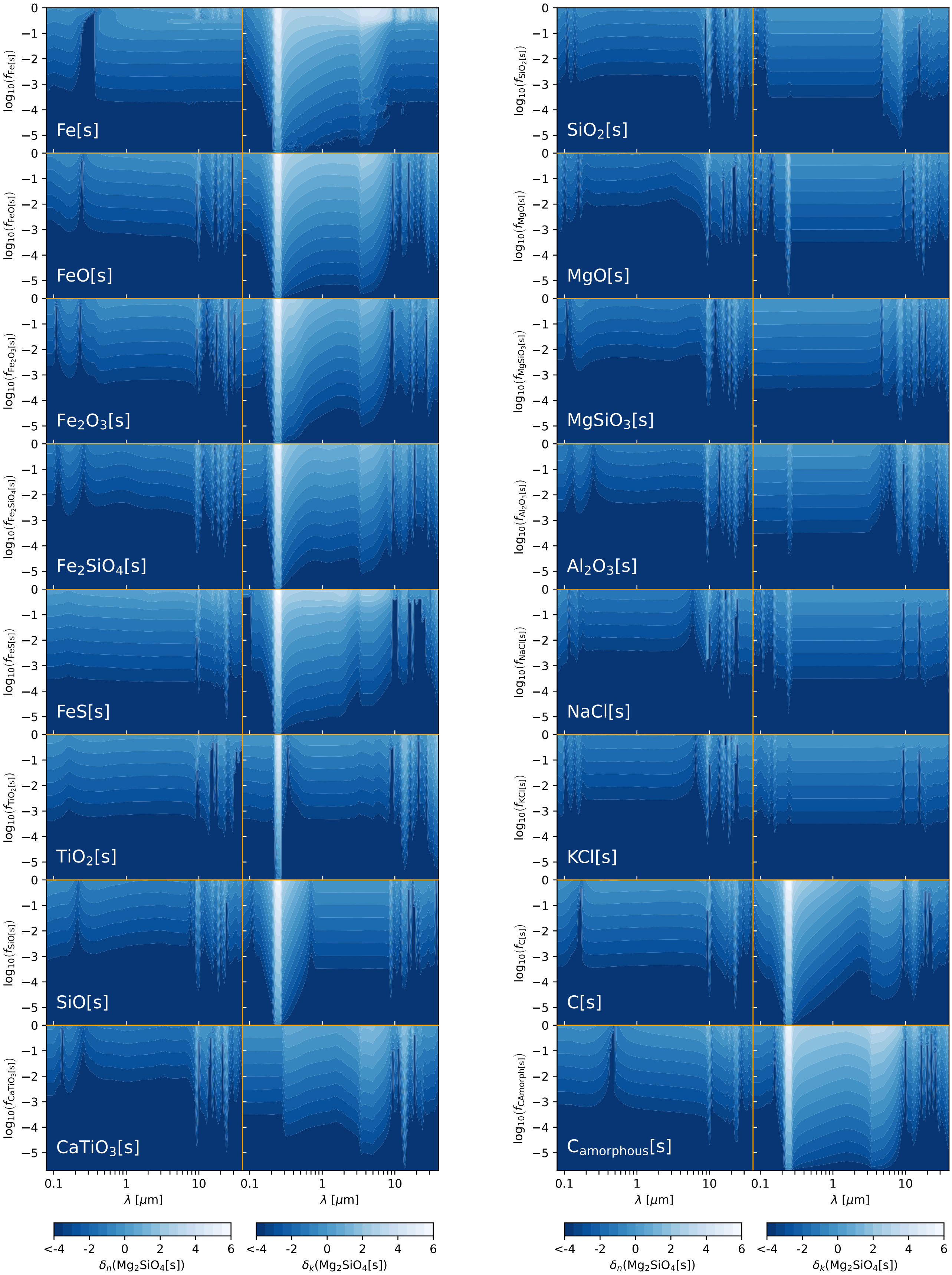

Fig. 3. Differences of the real and imaginary part of the refractive index (Eq. **??**) for two-component materials compared to the refractive index of Mg_2SiO_4[s] using Bruggeman. The first component is Mg_2SiO_4[s] and the second component is specified in each plot. **Left:** real part $n_{\rm eff}$. **Right:** imaginary part $k_{\rm eff}$.

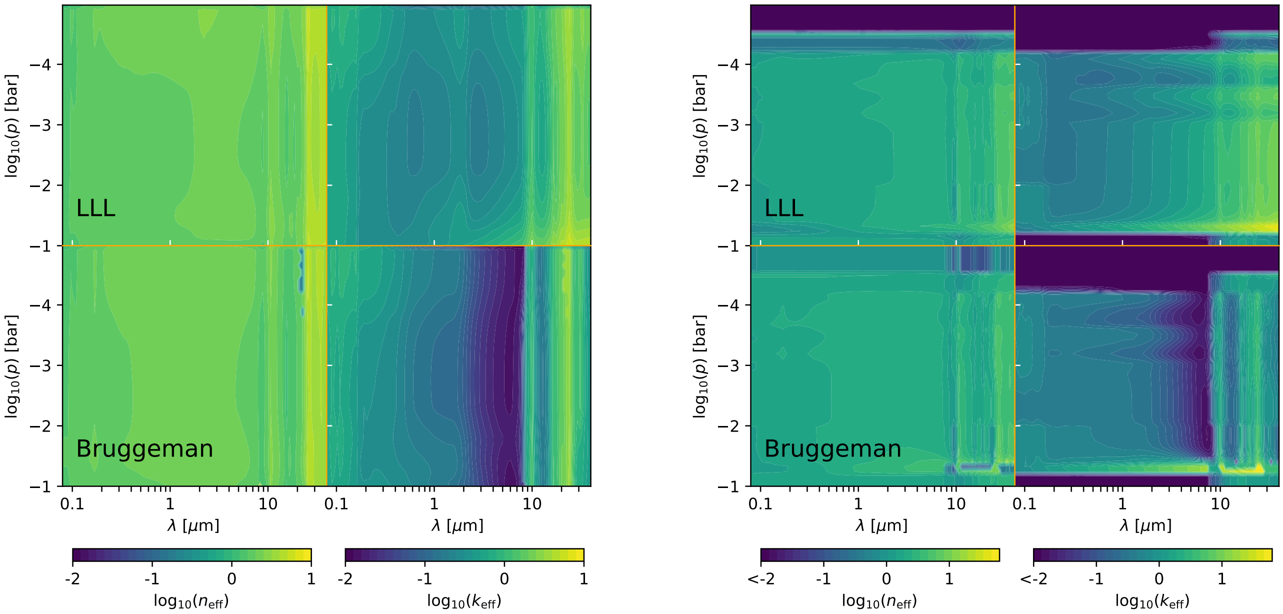

Fig. 4. Pressure dependent effective refractive index at the equator of the morning terminator. **Left:** HATS-6b. **Right:** WASP-76b.

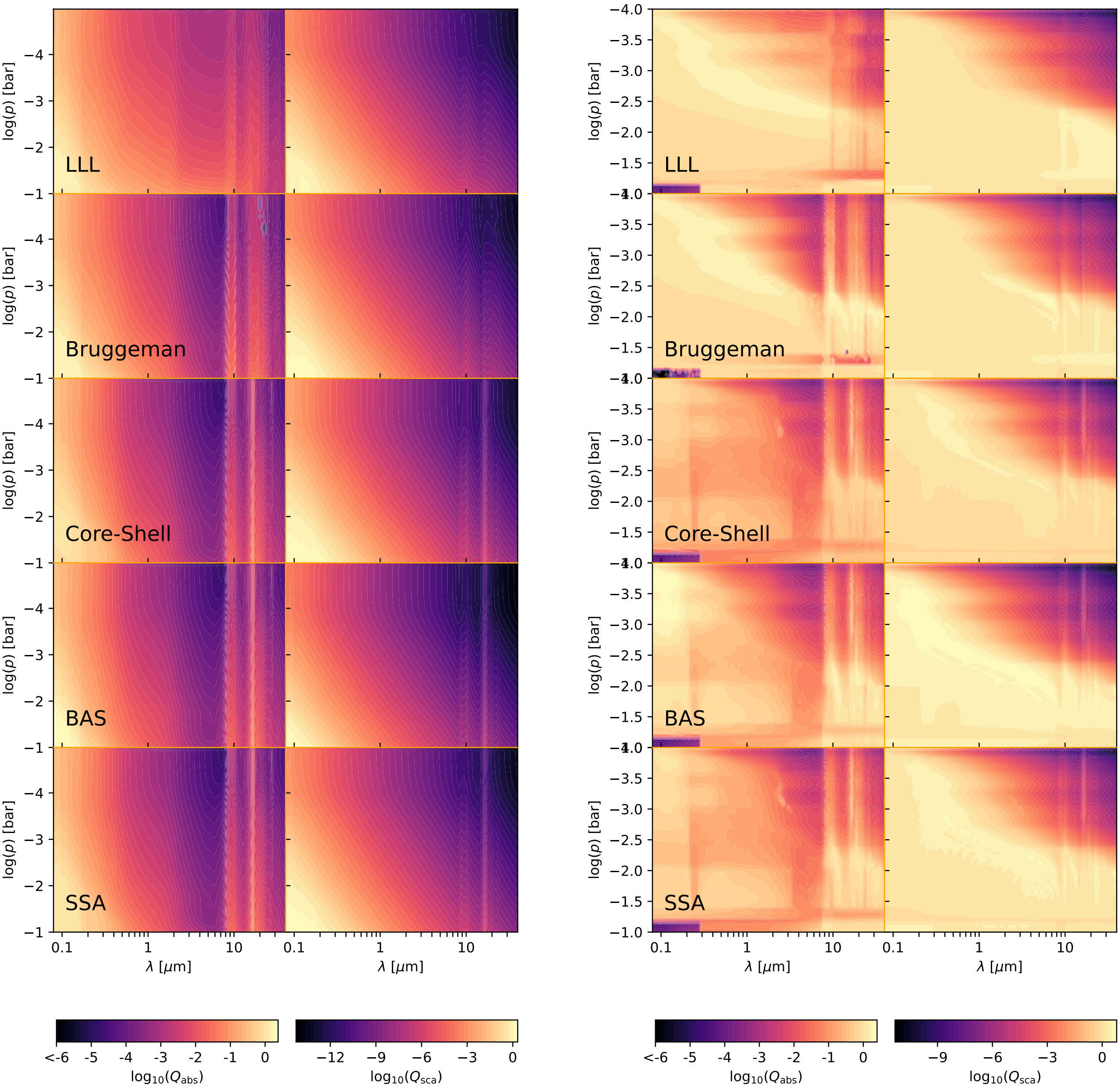

Fig. 5. Pressure dependent absorption and scattering efficiency at the equator of the morning terminator. **Left:** HATS-6b. **Right:** WASP-76b.

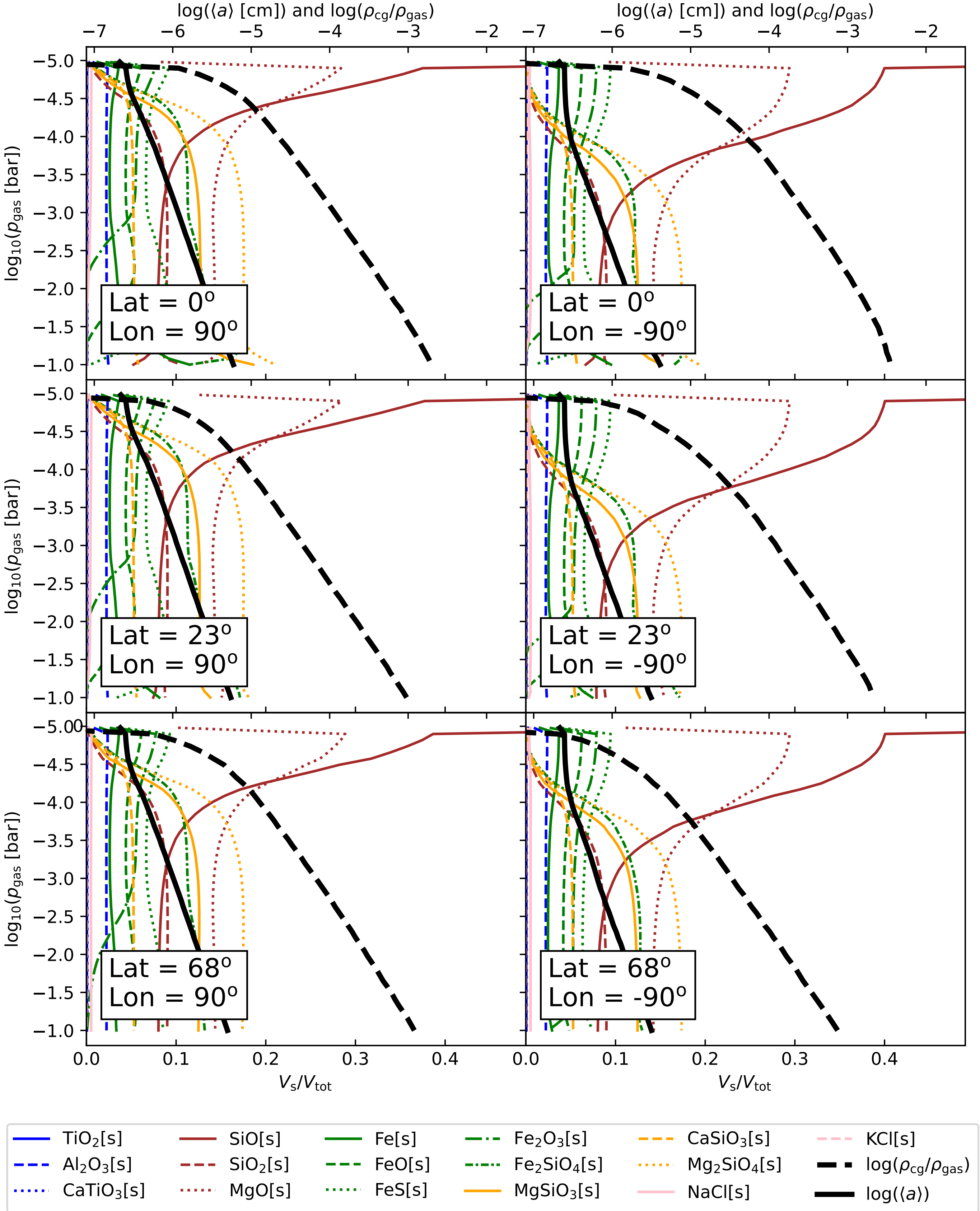

Fig. 6. Volume fractions V_s/V_{tot} of each cloud particle species considered (coloured lines), average cloud particle radius $\langle a \rangle$ of all cloud particles, and the total cloud mass fraction ρ_{cloud}/ρ_{gas} for HATS-6b. Data taken from Kiefer et al. (2024).

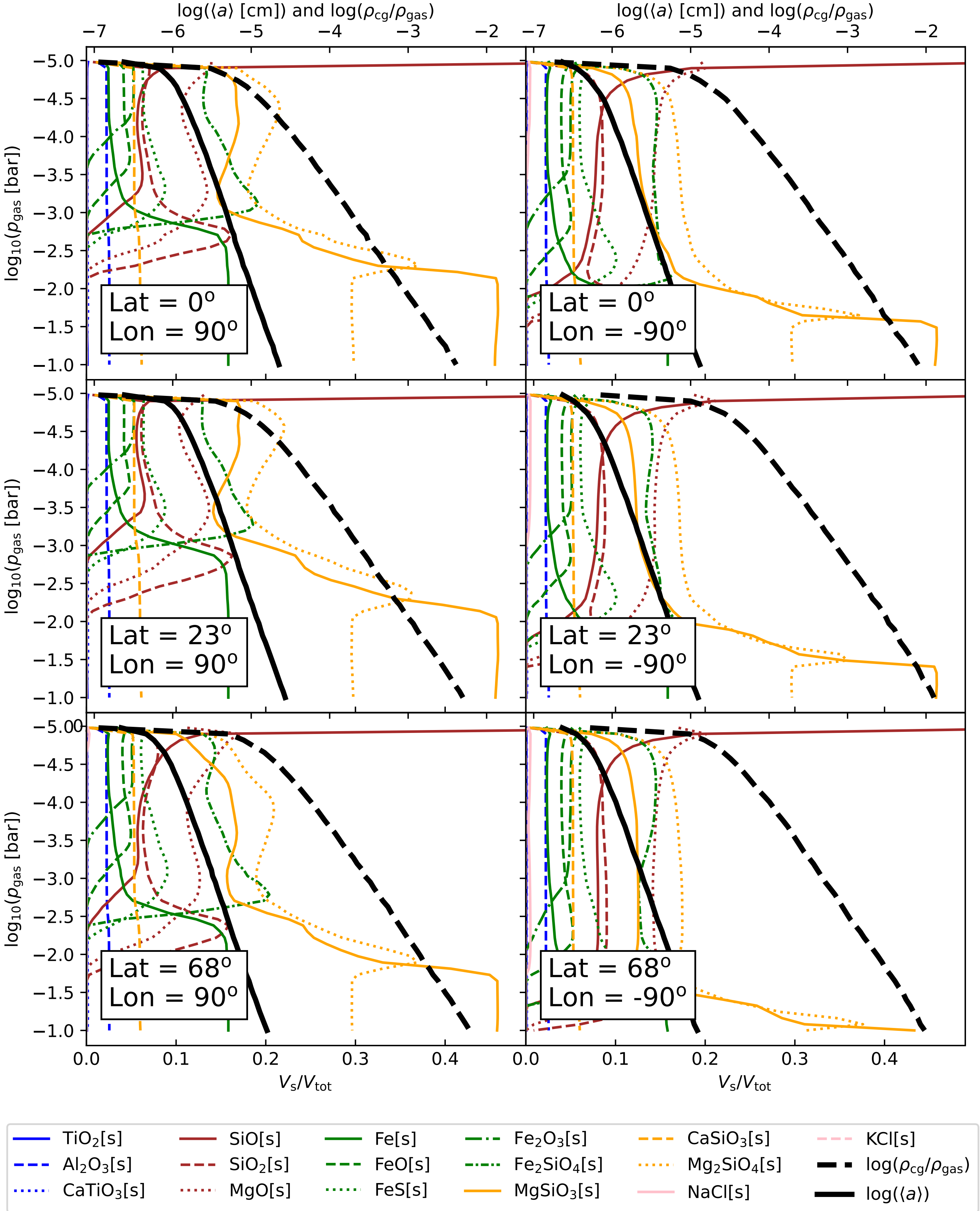

Fig. 7. Volume fractions V_s/V_{tot} of each cloud particle species considered (coloured lines), average cloud particle radius $\langle a \rangle$ of all cloud particles, and the total cloud mass fraction ρ_{cloud}/ρ_{gas} for WASP-39b. Data taken from Carone et al. (2023).

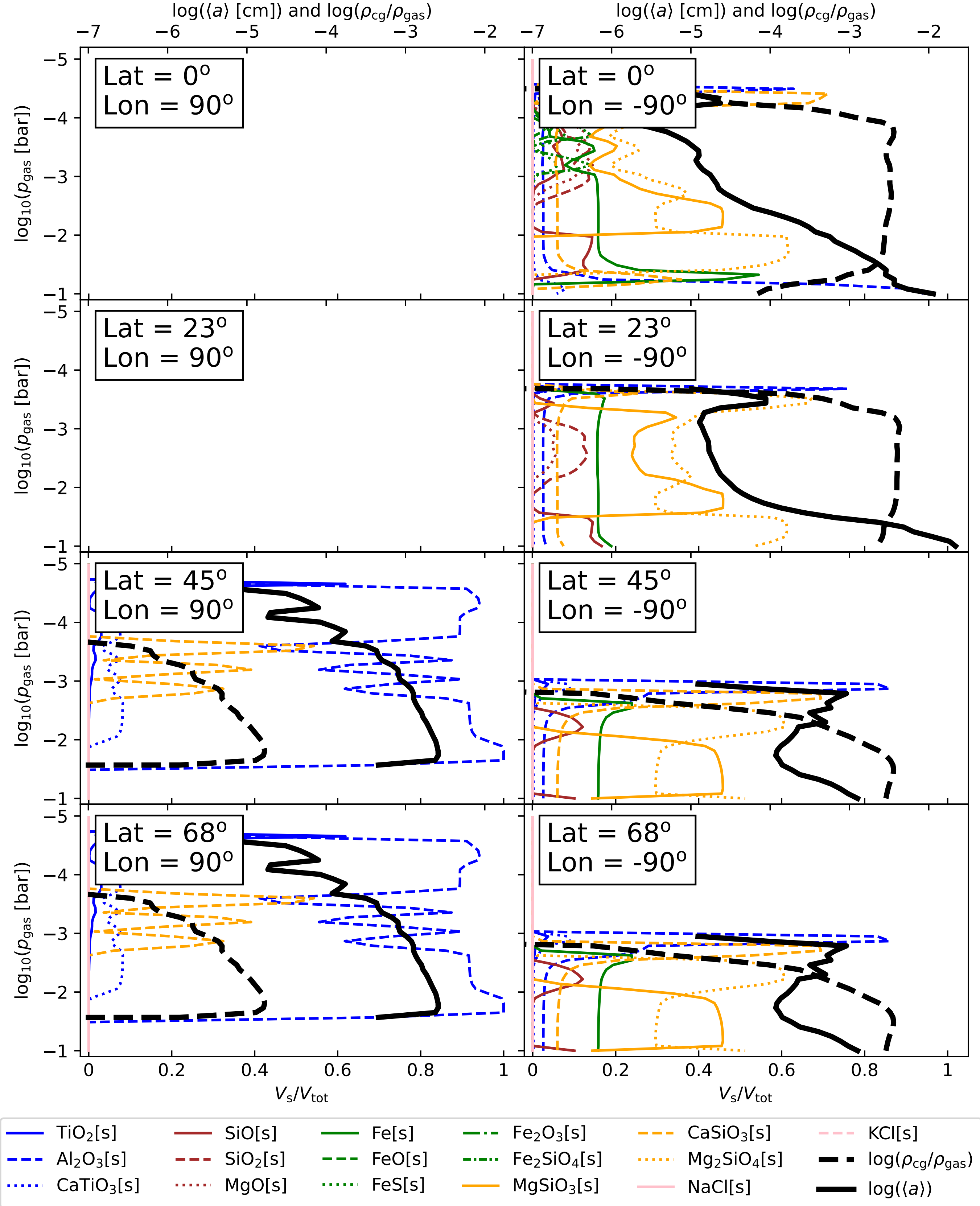

Fig. 8. Volume fractions V_s/V_{tot} of each cloud particle species considered (coloured lines), average cloud particle radius $\langle a \rangle$ of all cloud particles, and the total cloud mass fraction ρ_{cloud}/ρ_{gas} for WASP-76b. The evening terminator (lon = 90°) around the equator (lat = 0° and 23°) is cloud free.